

Composite Circumstellar Dust Grains

Ranjan Gupta^{1*}, Dipak B. Vaidya² and Rajeshwari Dutta¹

1. IUCAA, Post Bag 4, Ganeshkhind, Pune-411007, India

2. Gujarat College, Ahmedabad-380006, India

Received on 2016 April 25; Accepted on 2016 July 13

ABSTRACT

We calculate the absorption efficiencies of composite silicate grains with inclusions of graphite and silicon carbide in the spectral range 5–25 μm . We study the variation in absorption profiles with volume fractions of inclusions. In particular we study the variation in the wavelength of peak absorption at 10 and 18 μm . We also study the variation of the absorption of porous silicate grains. We use the absorption efficiencies to calculate the infrared flux at various dust temperatures and compare with the observed infrared emission flux from the circumstellar dust around some M-Type & AGB stars obtained from IRAS and a few stars from Spitzer satellite. We interpret the observed data in terms of the circumstellar dust grain sizes; shape; composition and dust temperature.

Key words: Circumstellar Dust: dust – infrared emission; stars: circumstellar matter

1 INTRODUCTION

In general, the composition of circumstellar dust around evolved stars are studied from observations in the near and mid-infrared spectroscopy of absorption and emission features. Emission from the characteristic 10 and 18 μm features, which arise from the bending and stretching modes of silicate grains, were first identified in the spectra of oxygen rich giants and super giants, Woolf & Ney (1969), Woolf (1973), Bode (1988). Little-Marenin & Little (1990) have analyzed about 450 IRAS-LRS spectra of M Mira variables to determine the morphology of the emission features, found near 10 μm and to correlate the shape of this feature with period, mass loss rates and other parameters of the stars. Simpson (1991) has analyzed the shape of the silicate dust features of 117 stars using spherical dust shell models. Evolved stars have distinctive IR spectra according to C/O abundance ratio e.g. Aitken et al. (1979), Cohen (1984). It is to be noted, however, that among the stars of the principal condensates in the two environments, amorphous carbon and silicates, only those with silicate environments have been detected directly. Amorphous carbon lacks strong IR resonances, although most of the continuum emission from carbon stars is presumably attributed arising from amorphous carbon, Groenewegen (1997). Silicon Carbide (SiC) emission at 11.3 μm is the only spectral feature of dust commonly observed in normal C-type red giants. However, as noted by Lorenz-Martins & Lefevre (1993), SiC

contributes only 10% or less of the dust in such objects. Although, the correlation between the C/O abundance ratio and the form of the IR spectrum is not perfect, the dust features are sometimes used as diagnostic of the C/O abundance ratios in stars. In some cases, silicate emission features are detected in stars classified as C rich e.g. Little-Marenin (1986), Waters et al. (1998). Their analysis indicates that the peak wavelength, strength and shape of the silicate features are very important to obtain the exact composition, sizes and shapes of the silicate grains. Thus, in order to interpret the observed silicate emission, we must compare the observed data with various silicate based models. In this paper, we have systematically analyzed the spectra of about 700 IRAS-LRS stars and compared them with composite dust grain models. We have also analyzed four other M-type & AGB stars observed by Spitzer satellite.

The grains flowing out of the stars are most likely to be non-spherical and inhomogeneous, porous, fluffy and composites of many very small particles due to grain-grain collisions, dust-gas interactions and various other processes. Further, observations from space and balloon probes show that, in general, dust grains are porous, fluffy and composites of many very small grains glued together, see Brownlee (1987); Köhler & Mann (2004); Lasue et al. (2009) and Levasseur-Regourd & Hadamcik (2013). Since there is no exact theory to study the scattering properties of these composite grains, various approximation methods are used for formulating models of electromagnetic scattering by these grains, such as EMA (Effective Medium Approximation), DDA (Discrete Dipole Approximation), etc. In EMA the

* E-mail: rag@iucaa.in

optical properties (refractive index, dielectric constant) of a small composite particle, comprising a mixture of two or more materials, are approximated by a single averaged optical constant and then Mie theory or T-Matrix is used to calculate absorption cross sections for spherical/non-spherical particles. Basically, the inhomogeneous particle is replaced by a homogeneous one with some average effective dielectric function. The effects related to the fluctuations of the dielectric function within the inhomogeneous structures cannot be treated by this approach. For details on EMA, refer to Bohren & Huffman (1983).

On the other hand, DDA takes into account irregular shape effects, surface roughness and internal structure of dust grains. DDA is computationally more rigorous than EMA. (For a discussion and comparison of DDA and EMA methods, including the limitations of EMA, see Bazell & Dwek (1990), Perrin & Lamy (1990), Perrin & Sivan (1990), Ossenkopf (1991) and Wolff et al. (1994). The DDA, which was first proposed by Purcell & Pennypacker (1973), represents a composite grain of arbitrary shape as a finite array of dipole elements. Each dipole has an oscillating polarization in response to both the incident radiation and the electric fields of the other dipoles in the array, and the superposition of dipole polarizations leads to extinction and scattering cross sections. For a detailed description of DDA, see Draine (1988). In an earlier paper by Vaidya & Gupta (2011), the effects of inclusions and porosities on the 10 and 18 μ m features were studied for the average observed IRAS spectra. In this paper, we use both DDA and EMA-T-Matrix to study the absorption properties of the composite grains consisting of host silicate spheroidal grains and inclusions of graphite or silicon carbide (SiC). The effects of inclusions and porosities, grain size and axial ratio (AR) on the absorption efficiencies of the grains in the wavelength range 5–25 μ m have been studied. In particular, we have systematically studied the 10 μ m silicate feature as a function of the volume fraction of the inclusions. Using the absorption efficiencies of these composite grains for a power law grain size distribution (Mathis et al. (1977)), the infrared fluxes for these grain models were calculated at various dust temperatures (T=200–400K). The infrared flux curves obtained from the models were then compared with the observed infrared emission curves of circumstellar dust around 700 oxygen-rich M-type and AGB stars, obtained by IRAS and Spitzer satellites. Kessler-Silacci et al. (2006) have used opacities for distribution of hollow spheres (DHS) of silicate shells Min et al. (2005) and these models have been compared with circumstellar dust around a few stars observed by Spitzer satellite. The DHS method averages the scattering and absorption/emission cross sections of the set of hollow spheres. Smolders et al. (2012) have used silicates and gehlenite to study the 10 and 18 μ m peaks in circumstellar dusts around S-type stars obtained by Spitzer satellite. Very recently, Siebenmorgen et al. (2014) have used a mixture of amorphous carbon and silicate dust models to interpret interstellar extinction, absorption, emission and polarization in the diffused interstellar medium. Mathis (1996) and Voshchinnikov et al. (2006) have used amorphous carbon with silicate in their composite grain model. Zubko et al. (2004) have reviewed various dust models including composite silicate-graphite grain model and they have used EMA-T-Matrix method to calculate ex-

tingtion efficiencies composite grains. Using T-Matrix based method, Iati et al. (2004) have studied optical properties of composite interstellar grains. Draine & Li (2007), have used silicate-graphite-PAH model to study the infra-red emission from interstellar dust in the post-Spitzer era. Using a radiative transfer model, Kirchschrager & Wolf (2014) have studied the effect of dust porosity on the appearance of protoplanetary disks.

A description of the composite grain models used is given in Section 2. In Section 3, the results of the studies on the absorption efficiencies of the grain models are presented. Section 4 provides results of the comparison of the model curves with the observed IR fluxes obtained by IRAS and Spitzer satellites. The conclusions are presented in Section 5.

2 COMPOSITE GRAIN MODELS

The absorption efficiencies Q_{abs} of composite grains, made up of a host silicate oblate spheroid and inclusions of graphite/silicon carbide and voids for porous silicate grains, for three axial ratios, in the spectral region 5–25 μ m, are computed using the DDA and EMA-T-Matrix methods. The details on these composite grain models using DDA are provided in Vaidya et al. (2007), Vaidya & Gupta (2009) and Vaidya & Gupta (2011).

We have selected oblate (axial ratio > 1) spheroid since, it provides a good fit to the observed polarization across the 10 μ m feature Henning & Stognienko (1993), Kim & Martin (1995). Earlier, Draine & Lee (1984) have also used oblate silicate spheroids to model interstellar grains. Gupta et al. (2005) have also shown that the interstellar extinction curves obtained with oblate spheroidal grain models fit best with the observed interstellar extinction.

Discrete Dipole Approximation (DDA) based grain models:

Composite spheroidal grain models containing N (number of dipoles) = 9640, 25896 and 14440 dipoles (corresponding to axial ratios AR = 1.33, 1.5 and 2.0 respectively), each carved out from $32 \times 24 \times 24$, $48 \times 32 \times 32$ and $48 \times 24 \times 24$ dipole sites respectively are used. Sites outside the spheroid are set to be vacuum and sites inside are assigned to be the host material. The size of the inclusion is given in terms of the number of dipoles 'n' across the diameter of an inclusion, e.g. n = 152 dipoles for composite grain model with N = 9640, i.e. AR = 1.33 and volume fraction of f=0.1. Please see Table 1 in Vaidya & Gupta (2011) and also Chýlek et al. (2000). The DDA code generates a three dimensional matrix, specifying the material type at each dipole site. There are two validity criteria for DDA (see e.g. Wolff et al. (1994)); viz. (i) $|m|kd \leq 1$, where m is the complex refractive index of the material; $k=\pi/\lambda$ is the wavenumber and d is the lattice dispersion spacing and (ii) d should be small enough (N should be sufficiently large) to describe the shape of the particle satisfactorily. For all the composite grain models, viz. N=9640; 14440 & 25896; and for all grain sizes 0.005-0.250 μ in the wavelength range 5–25 μ m considered in the present study, we have checked that the DDA validity criteria are satisfied. Details on the computer code and the corresponding modification to the DDSCAT 6.1 code Draine & Flatau

(2003) are given in Vaidya et al. (2001) and Gupta et al. (2005).

Effective Medium Approximation (EMA-T-Matrix) based models:

We have also obtained absorption efficiencies for composite grains using the combination of EMA-T-Matrix calculations. In EMA, a mixing rule (e.g. Maxwell-Garnet or Bruggman see: Bohren & Huffman (1983)) is used to obtain the average refractive index (by using the optical constants of two materials) of the composite grain. We have used Maxwell-Garnet mixing rule. The absorption efficiencies of the composite grains are calculated using the T-Matrix code given by Mishchenko et al. (2002). Earlier, Gupta et al. (2005) and Vaidya & Gupta (2009) have used EMA-T-Matrix based method to study scattering properties of composite grains. For a discussion on various EMA mixing rules see Bohren & Huffman (1983).

Grain size and size distribution:

We have used the power-law MRN, Mathis et al. (1977), dust grain size distribution:

$$n(a) \propto a^{-q} (a_{\min} < a < a_{\max}),$$

where a is the effective radius. This law states that the number of dust grains per unit volume having radius between a and $a + da$, is proportional to a^{-q} . An acceptable fit to the observed data is obtained with values of $a_{\min} = 0.005\mu$, $a_{\max} = 0.250\mu$ and $q = 3.5$. If the semi-major and semi-minor axes are denoted by $x/2$ and $y/2$ respectively, then $a^3 = (x/2)(y/2)^2$, where 'a' is the radius of the equivalent sphere, whose volume is the same as that of the spheroid.

Types of Inclusions:

For the composite grain models, we have used the host silicate spheroid with graphite or silicon carbide (SiC) inclusions. Graphite is selected as inclusions, since it explains the observed bump at 2175\AA in the UV region of the extinction curve Draine (1988). O'Donnell (1994) and Henning & Stognienko (1993) have also used graphite inclusions in the composite grain models. Min et al. (2007), Min et al. (2008) have used SiC as inclusions to study the $10\mu\text{m}$ silicate feature.

We have also used porous silicate grain models, as the circumstellar grains are likely to be porous and fluffy, Köhler & Mann (2004) and Voshchinnikov et al. (2005).

The complex refractive indices for silicates and graphite were obtained from Draine (2003). The optical constants for SiC were obtained from Pegourie (1988). The volume fractions of the inclusions are denoted as $f = 0.04, 0.06, 0.08, 0.1, 0.2$ & 0.30 etc.

Orientation:

For randomly oriented spheroidal grains, the scattering properties of the composite grains have to be averaged over all of the possible orientations. In the present study, we have used three values for each of the orientation parameters and averaging is done over 27 different orientations for all DDA computations (see Wolff et al. (1994) & Wolff et al. (1998)).

For an illustration of a composite grain model with $N = 14440$ (total 14440 dipoles with 11 inclusions of 224 dipoles per inclusion); see Fig.1a and Fig1b.

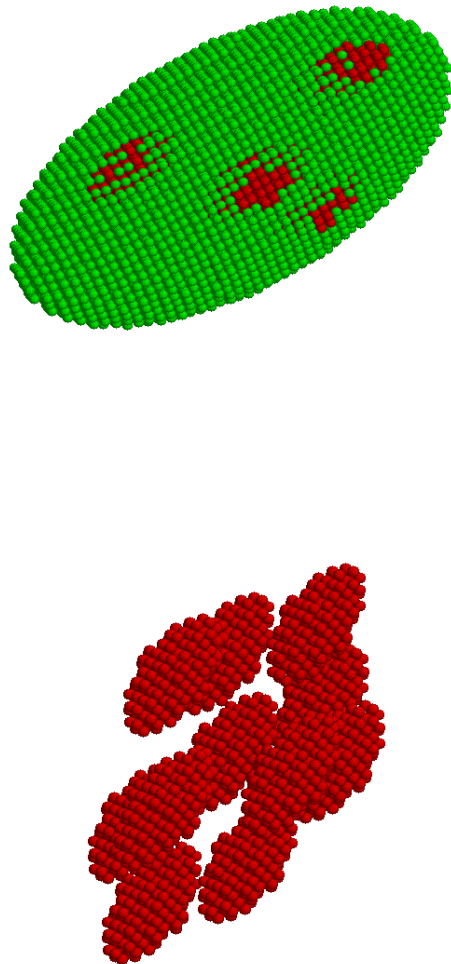


Figure 1. Figure 1a(top): A non-spherical composite dust grain consisting of host (in green) and inclusion (in red) with a total of $N=14440$ dipoles where the 11 inclusions are embedded in the host spheroid are shown such that only the ones placed at the outer periphery are seen in this panel. Figure 1b(bottom): The 11 inclusions are shown separately in this panel (somewhat enlarged than Fig. 1a).

3 MODEL ABSORPTION CURVES AND ABSORPTION EFFICIENCY OF COMPOSITE GRAINS

We have calculated the absorption efficiencies for the composite grain models with spheroidal silicates as host and graphite/or silicon carbide inclusions. The composite grain models with graphite inclusions have been used earlier by Ossenkopf (1991), O'Donnell (1994), Henning & Stognienko (1993), Vaidya & Gupta (2011) and with SiC by Kessler-Silacci et al. (2006), Min et al. (2008) and Siebenmorgen et al. (2014). We have also calculated the absorption efficiency for the porous silicate grains. Porosity

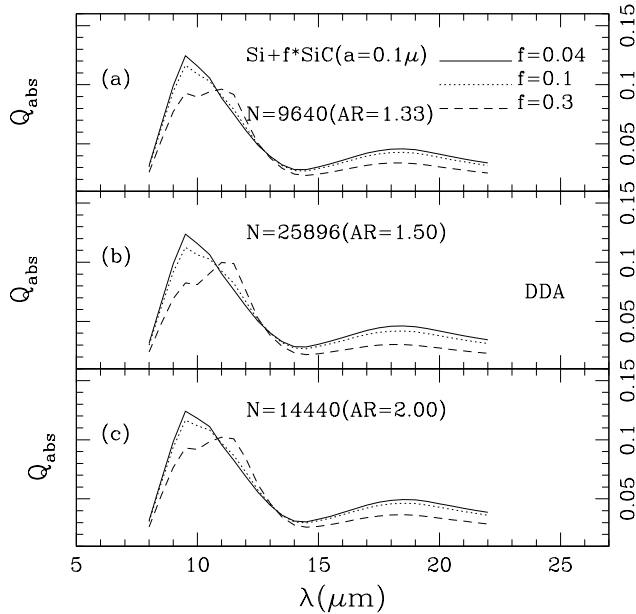


Figure 2. Variation in Q_{abs} with SiC inclusions for three axial ratios and grain size 0.10μ over wavelength range 5-25 μm using DDA calculations.

'P' is defined as $P = 1 - V_{\text{solid}}/V_{\text{total}}$; where V_{solid} is the number of dipoles of the material and V_{total} is the total number of dipoles in the spheroid; accordingly the porosity varies from 1–30% for the spheroidal grains (Greenberg (1990) and Vaidya & Gupta (1997)). Earlier, porous silicate grains have also been used by Li et al. (2008) for modeling the dust around AGN stars. Voshchinnikov et al. (2013) have studied the effect of porosities on the $10\mu\text{m}$ silicate feature. Using Köhler & Mann (2004), have calculated radiation pressure cross-sections on porous (porosities 30–90%) astronomical spherical silicate grains in the circumstellar dust shells around β -Pictoris, Vega & Formalhaut stars. Köhler & Mann (2004) have also used the combination of EMA and Mie theory and calculated the radiation pressure cross-sections of porous silicate grains and compared with the DDA results. They have also noted that the DDA method is time consuming.

The variation in absorption efficiencies Q_{abs} of the composite grains with different volume fractions (0.04, 0.10,...0.3) of the inclusions of Silicon Carbide (SiC) for the three different axial ratios 1.33, 1.5 and 2.0, in the wavelength range 5–25 μm for the grain size $a = 0.10\mu$ is shown in Figs. 2(a, b & c). It is seen that for the composite grain models with inclusions of SiC, the strength of both the 10 and 18 μm absorption peaks decreases with increase in the volume fractions. It is to be noted that for higher volume fractions 0.3 of SiC inclusions, the the 10 μm feature is modified considerably.

We have also computed absorption efficiencies of the composite grains using EMA-T-Matrix based calculations. In Figs. 3(a, b & c), we show the absorption profiles of composite grains with three SiC inclusions. It is seen that the absorption efficiencies increase with volume fraction of SiC and there is no appreciable shift in the wavelength of peak absorption at 10 μm feature. In our earlier study

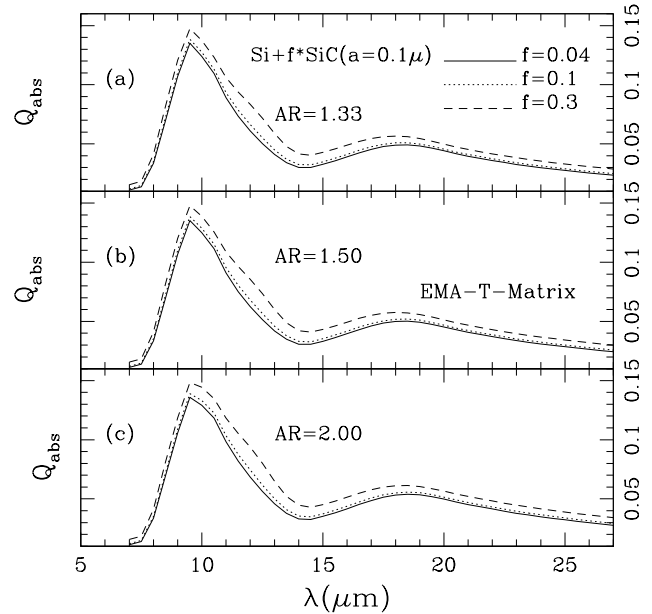


Figure 3. Variation in Q_{abs} with SiC inclusions for different axial ratios (AR) and grain size 0.10μ over wavelength range 5–25 μm , using EMA-T-Matrix calculations

Vaidya & Gupta (2011), using DDA, we have shown the variation of absorption efficiencies of composite grains with inclusions of graphite and porous silicate grains.

In Fig.4, we compare the absorption efficiencies of the composite grains with inclusions of graphite and porous grains obtained using DDA and EMA-T-Matrix methods. It is seen in Fig 4 (a) & (c) the absorption efficiencies decrease as the volume fractions of graphite increases for both DDA & EMA-T-Matrix. The absorption efficiencies for porous silicate grains as seen in Fig. 4 (b) for DDA decreases with increasing inclusion fraction whereas for EMA-T-Matrix in 4 (d) there is no appreciable change. Figure 5 shows how the ratio between Q_{abs} calculated from DDA and EMA-T-Matrix deviate and it clearly shows that for higher volume fractions, the ratio deviations are more prominent around the 15 μm region.

The absorption efficiencies obtained using EMA-T-Matrix calculations and DDA do not agree because the EMA method does not take into account the inhomogeneities within the grains (internal structure, surface roughness etc see Wolff et al. (1998) and the material interfaces and shapes are smeared out into the homogeneous 'average mixture'; thus the refractive index using EMA is an average one and the resulting absorption efficiency is not reliable, Saija et al. (2001). However, EMA-T-Matrix method is still quite useful since the application of DDA poses a computational challenge for large size parameter $X = 2\pi a/\lambda > 20$ and large complex refractive index m . Further, EMA allows to examine applicability of several mixing rules see e.g. Wolff et al. (1998); Chýlek et al. (2000); Saija et al. (2001); Voshchinnikov et al. (2005) and Voshchinnikov et al. (2006).

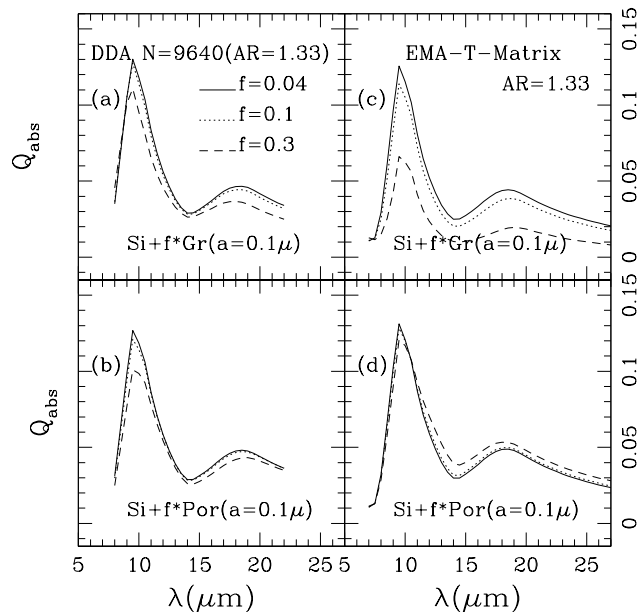


Figure 4. Absorption efficiencies of composite grains with graphite inclusions (a) & (c) & porous silicates (b) & (d), using DDA & EMA-T-Matrix methods

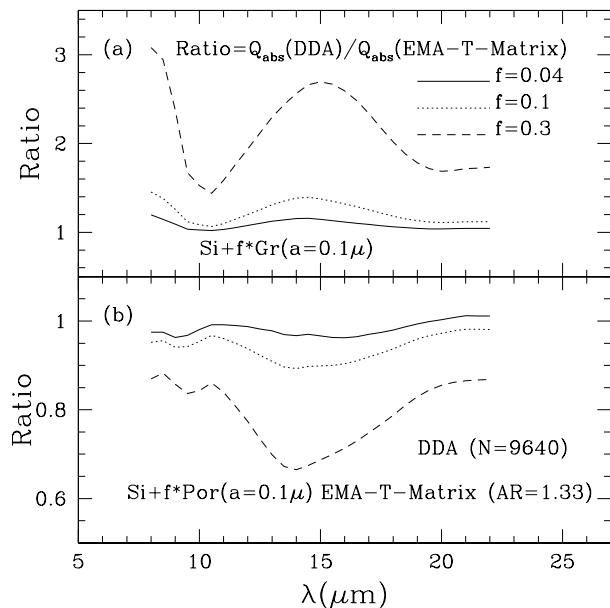


Figure 5. Ratio of Absorption efficiencies of composite grains with graphite inclusions (panel (a)) & porous silicates (panel (b)), using DDA & EMA-T-Matrix methods

4 IR EMISSION FROM DUST AND COMPARISON WITH OBSERVED DATA

The stars which have evolved from the main sequence and have entered the giant phase of their evolution are a major source of dust grains in the galactic interstellar medium. Such stars have oxygen-rich material (e.g. olivine) over abundant relative to carbon, and therefore, produce silicates and show strong feature at $10\mu\text{m}$. The $10\mu\text{m}$ feature is

identified with the Si-O bond, from stretching mode. These materials (amorphous silicates, e.g. olivines and pyroxenes) also show a weaker feature at $18\mu\text{m}$ resulting from O-Si-O bending mode, Little-Marein & Little (1990) and Whittet (2003). These features can be present in either emission or absorption spectra depending on the optical depth of the circumstellar shell.

The Infrared Astronomical Satellite (IRAS) had an instrument called the Low Resolution Spectrometer (LRS), which measured spectra of the brighter ($> 10\text{Jy}$) point sources (about 50,000), between 7.7 and $22.6\mu\text{m}$, with a resolution varying from 20 to 60. A total of 5425 objects with better quality spectra were included in the Atlas of Low-Resolution IRAS Spectra, Olmon et al. (1986). Two thousand bright sources from the Atlas were classified into 17 different classes based on their spectral morphology using Artificial Neural Network (ANN) scheme Gupta et al. (2004). Objects belonging to Class 6 of this classification, which are O-rich AGB stars with strong silicate emission feature at $10\mu\text{m}$, are considered for this paper. This class contains the largest number of objects (732) amongst all the classes.

Using the absorption efficiencies Q_{abs} of the composite grains, the infrared flux, F_{λ} at various dust temperatures is calculated using the relation, $F_{\lambda} = Q_{\text{abs}}B_{\lambda}(T)$ at dust temperature T in K, and B_{λ} is the Planck function. This relation is valid only if the silicate emission region is optically thin, Simpson (1991), Ossenkopf et al. (1992), & Li et al. (2008). It is also assumed that the dust is isothermal and the grains behave as perfect black bodies. As mentioned earlier in Section 2, we have used a MRN (power law) grain size distribution with $a_{\text{min}} = 0.005\mu$ and $a_{\text{max}} = 0.250\mu$, Mathis et al. (1977) for all the composite grain models to compare the observed IR fluxes. The composite grain model with larger grain size distribution in the range $a=0.1$ to 1.0μ did not match the observed curves satisfactorily. As noted by Sylvester et al. (1996), Telesco & Knacke (1991), Backman et al. (1992), Li & Greenberg (1998), Krivov et al. (2000) and Carciofi et al. (2004), small grain sizes are expected from the IR data and the profile of the silicate emission at $10\mu\text{m}$. In Figure 6, we show the variation of the infrared flux for a temperature range of 200–400K for composite grains with 10% SiC inclusions, and size integration of grain sizes from 0.005 to 0.250μ by both DDA and EMA-T-Matrix methods. It is seen that the flux decreases as the dust temperature increases.

The observed IRAS-LRS curves obtained for circumstellar dust around 700 oxygen rich M-type stars, are compared with the calculated infrared fluxes, F_{λ} , for the composite grain models. χ^2 minimization method is used to fit the observed data with the calculated infrared fluxes for the composite grain models. For details on the χ^2 method see Vaidya et al. (2007) & Vaidya & Gupta (2011). An error bar of 10% on the data is used, Olmon et al. (1986). In Fig. 7 histogram, we show the number of stars with the absorption band at $10\mu\text{m}$. It is seen that the maximum number of stars have peak wavelength range between 9.4 & $9.8\mu\text{m}$.

The best fit dust temperature is computed for each star along with the errors in temperature over a confidence level of 90%.

Some of the best fit infrared emission flux curves, for the composite grain models are shown in Fig. 8 with graphite; porous and SiC inclusions & porous silicate grains. The

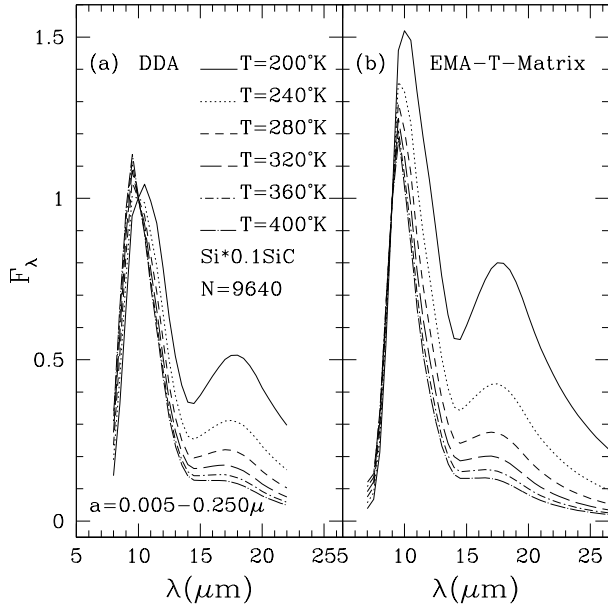


Figure 6. Infrared flux at various temperatures for composite grains with SiC inclusions.

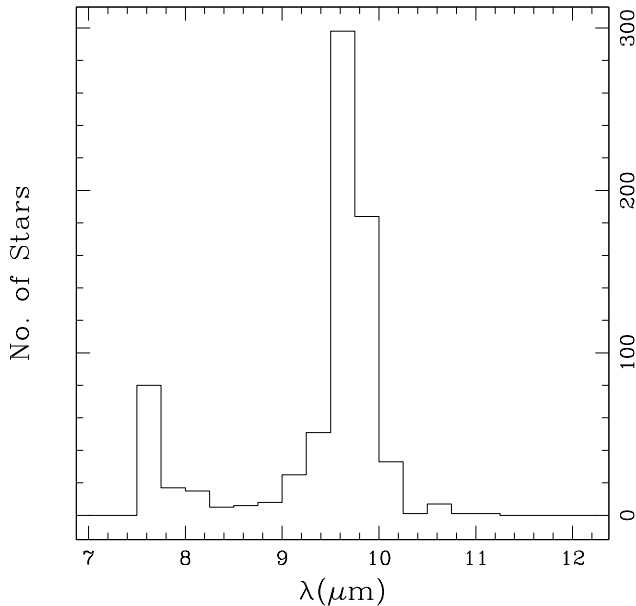


Figure 7. Histogram showing the statistics of the $10\mu\text{m}$ feature's variation amongst the 700 IRAS objects.

smooth curves represent the model data, while the points with error bars represent the observed data. The axial ratio and the dust temperature for the best fit grain model are also shown in the plots.

We also compare the observed IRAS-LRS flux data with best fit models using EMA-T-Matrix calculations in Fig. 9.

Table 1 shows the detailed parameters for composite grain and porous silicate grain models for some of the best fits of these models to a set of 10 IRAS stars, each with their IRAS catalogue No.; corresponding LRS No.; the best fit

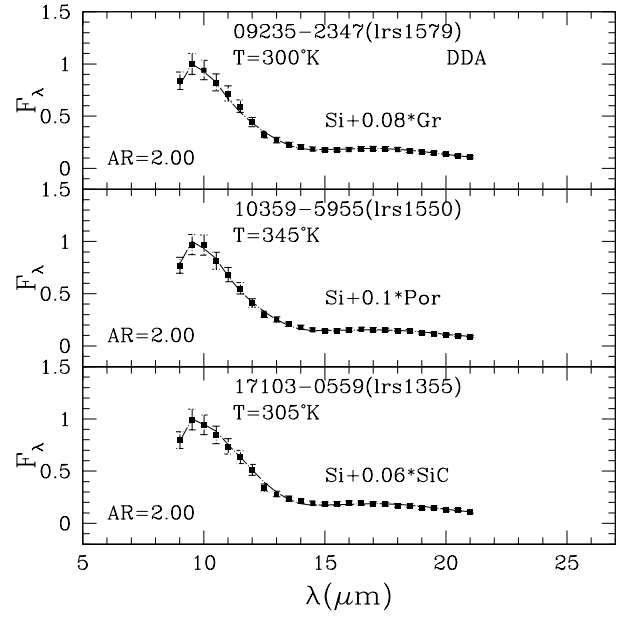


Figure 8. Composite grain models (DDA) with various inclusions fits to IRAS-LRS data. The number at top of each panel is the IRAS identifier.

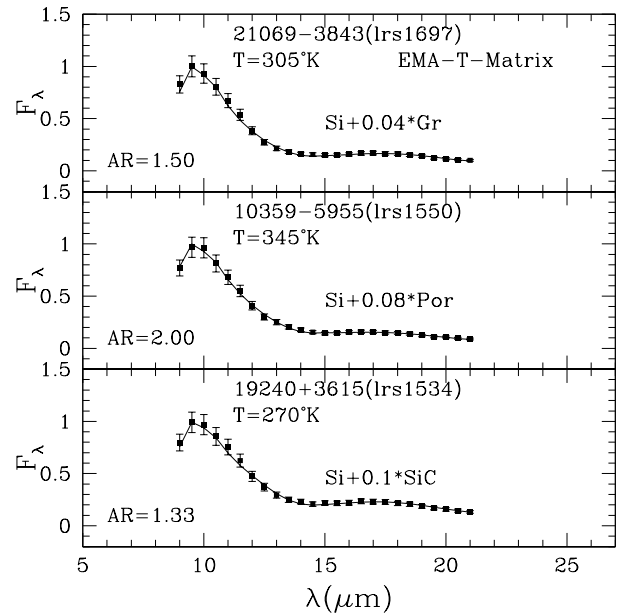


Figure 9. Composite grain models (EMA-T-Matrix) with various inclusions fits to IRAS-LRS data. The number at top of each panel is the IRAS identifier.

minimum χ^2 value; estimated temperature; model evaluated flux ratio ($R = \text{Flux}(18\mu) / \text{Flux}(10\mu)$); observed flux ratio (R) and the corresponding best fit DDA model. Table 2 shows the best fit results with EMA-T-Matrix model.

The results in Figs. 8 & 9, and Tables 1 & 2, show that the composite grain models with graphite inclusions fit the observed fluxes reasonably well, whereas the porous silicate models and the composite grain models with inclusions of

Table 1. List of best χ^2 fit DDA based models to the IRAS objects – a list of best selected 10 stars. The best fit model notation e.g. 2.00si0.08gr denotes that the axial ratio (AR) is 2 and si0.08gr denotes 8% volume inclusion of graphite in the host silicate grain.

IRAS No.	LRS No.	Min. χ^2	T(K)	Model R	Obs.R	BestFitModel
09235-2347	lrs1579	0.1515	300.0	0.180	0.180	2.00si0.08gr
17119+0859	lrs1915	0.1710	285.0	0.202	0.203	2.00si0.08gr
10359-5955	lrs1550	0.1863	345.0	0.146	0.149	2.00si0.1por
20484-7202	lrs1670	0.1905	295.0	0.186	0.176	2.00si0.1gr
18595-3947	lrs1975	0.1963	290.0	0.182	0.173	2.00si0.3gr
19240+3615	lrs1534	0.2002	275.0	0.218	0.213	2.00si0.1gr
19244+1115	lrs1992	0.2057	220.0	0.390	0.379	2.00si0.2gr
11525-5057	lrs1482	0.2189	295.0	0.187	0.178	2.00si0.08gr
16340-4634	lrs1946	0.2208	265.0	0.232	0.234	2.00si0.2gr
06297+4045	lrs1617	0.2225	260.0	0.244	0.244	2.00si0.2gr

Table 2. List of best χ^2 fit EMA-T-Matrix based models to the IRAS objects – a list of best selected 10 stars. The best fit model notation e.g. 2.00si0.08por denotes that the axial ratio (AR) is 2 and si0.08por denotes 8% volume inclusion of vacuum in the host silicate grain making it a porous silicate grain.

IRAS No.	LRS No.	Min. χ^2	T(K)	Model R	Obs.R	BestFitModel
10359-5955	lrs1550	0.1500	345.0	0.146	0.149	2.00si0.08por
09235-2347	lrs1579	0.1887	310.0	0.180	0.180	2.00si0.08por
17119+0859	lrs1915	0.2043	285.0	0.205	0.203	1.50si0.08por
02351-2711	lrs1884	0.2160	330.0	0.159	0.156	2.00si0.08por
19240+3615	lrs1534	0.2405	270.0	0.222	0.213	1.33si0.1sic
11525-5057	lrs1482	0.2429	295.0	0.190	0.178	1.50si0.08por
17484-0800	lrs1712	0.2495	315.0	0.174	0.166	2.00si0.08por
15255+1944	lrs1764	0.2528	290.0	0.194	0.194	1.33si0.08por
08124-4133	lrs1734	0.2544	295.0	0.191	0.188	1.50si0.3sic
21069-3843	lrs1697	0.2556	305.0	0.162	0.164	1.50si0.04gr

SiC do not fit the observed curves satisfactorily, as indicated by the χ^2 values.

Further, these results indicate that the temperature range of 250–350K derived from the grain models give satisfactory fit to the observed data. Stars giving good fits with the composite grain models with graphite & SiC inclusions have temperatures between 270 and 300K, while those with the porous silicate grain models give the best fit dust temperature between 300 and 370K. The estimated temperature errors are within 10K.

We have also used the data from the Infrared Spectrograph IRS (Houck et al. (2004)); on board the Spitzer Space Telescope, Werner et al. (2004) and extracted the spectrum of four M-type and AGB stars using the Cornell Atlas of Spitzer/IRS Sources (CASSIS) extraction procedure (Lebouteiller et al. (2015)). Figure 10 shows model fits with observed Spitzer data in the spectral range of 8–13 μ m for M-type stars and one AGB star (see Manteiga et al. (2011)). It is seen that the composite grain models or porous silicate grain models do not fit the observed Spitzer fluxes satisfactorily. The derived temperature range in these objects is around 220–250K. The stars in panels (a) and (b) fit to the composite grains with graphite inclusions and porous silicates respectively whereas the stars in panels (c) and (d) show the best fit to the composite grain models with SiC inclusions and seem to have been affected by the SiC feature at 11.3 μ m. Smolders et al. (2012) have used silicate grains with gehlenite grain models to fit the observed spectra of a few stars obtained by Spitzer, and have also noted that

grain models with a component of SiC are not suitable to fit the M-type stars. We note here that we need to analyze larger sample of M-type and AGB stars observed by Spitzer satellite.

Min et al. (2008) have used grain models with mixture of SiC and Si to interpret the observed 10 μ m absorption band and they have noted that the shape of SiC resonance is very sensitive to the shape of the SiC grain in the region of 10 μ m band. In Figs. 11 (a), (b) & (c) we show the effect of grain shape (axial ratio AR) on the silicate and SiC features at 10 and 11.3 μ m respectively. It is seen that the 10.0 μ m silicate feature is not affected by the grain shape, whereas, 11.3 μ m SiC feature shows variation with the grain shape (see Fig. 11 b & c).

Flux Ratio R in the Silicate Emission:

We have also calculated the flux ratio $R = \text{Flux}(18\mu) / \text{Flux}(10\mu)$ for all the composite grain models.

In our earlier study Vaidya & Gupta (2011), we had shown that, in general, the flux ratio R decreases with the dust temperature for the composite grains with graphite inclusions and porous silicate grain models, it varies between ~ 0.6 at 200K and 0.2 at 300K. We had also shown that for the composite grain models with graphite inclusions, the ratio R decreases with the volume fraction of the inclusions, whereas it increases with the porosities. Henning & Stognienko (1993) did not find any variation either with graphite inclusions or with the porosities. In Tables 1, 2 & 3, we show the flux ratio for the best fit models.

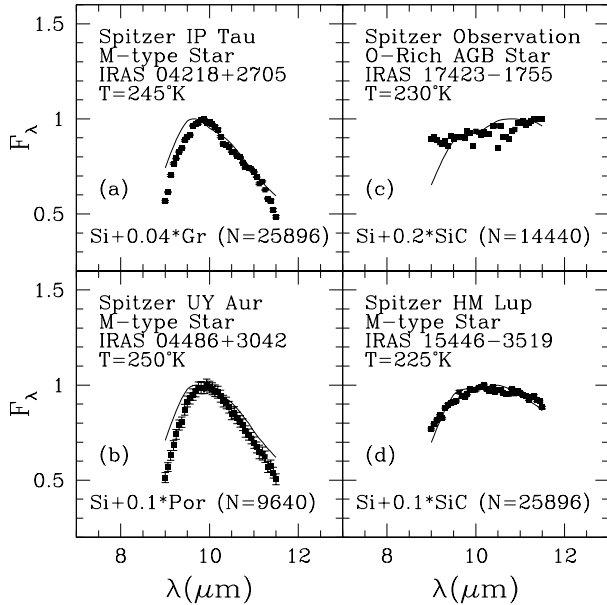


Figure 10. Best fits to a set of Spitzer observed spectra. The solid points with error bars are the Spitzer data and continuous line is the best fit model.

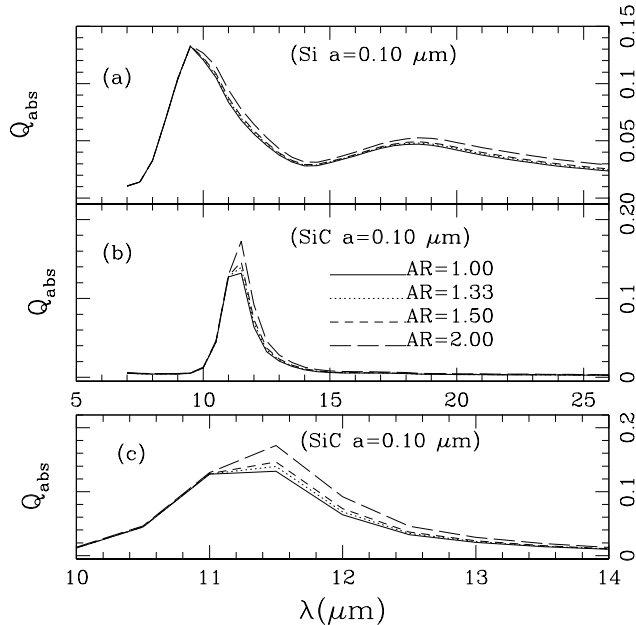


Figure 11. The panels (a) and (b) show the absorption efficiencies Q_{abs} at various axial ratios (AR) for Silicates (Si) and Silicon Carbide (SiC). The x-axis for both these panels is wavelength λ in (μm). The panel (c) is same as (b) but with the wavelength axis expanded to highlight the variation in the shape of the peak absorption feature of SiC at $11.3\mu\text{m}$ with the grain shape (i.e. AR).

In this paper, we also show R for the composite grains with SiC inclusions as depicted in Table 3. It is seen that the R decreases with the dust temperature which is consistent with the earlier results on composite grains with graphite inclusions and porous silicate grains, Vaidya & Gupta (2011). We also note that R obtained by EMA-T-Matrix is higher than that obtained by DDA.

5 CONCLUSIONS

In order to interpret dust properties (viz. sizes, shapes, composition and temperature) in circumstellar dust, we have systematically analyzed the IR spectra of about 700 IRAS-LRS oxygen rich M type stars using the composite grain models with graphite and silicon carbide (SiC) inclusions and porous silicate grain models. The $10\mu\text{m}$ band has been studied in more details and is compared with the observed data for the stars with the absorption band between 9.5 and $10.0\mu\text{m}$. It should be noted here that we have used both DDA & EMA-T-Matrix methods to compute the absorption efficiency of composite grain models and porous silicate grain models, whereas most of others have used EMA and T-Matrix methods or methods using Distribution of Hollow Spheres (DHS), Min et al. (2008) and Kessler-Silacci et al. (2006) or layered spheres method Mathis (1996).

The main conclusions are presented below:

(1) The absorption/emission properties of the silicate grains are modified considerably with the inclusions of carbonaceous materials (e.g. graphite & SiC) and porosity. Our results on the composite grain models clearly show the variation in absorption efficiency Q_{abs} with the variation of volume fraction of inclusions (graphite & SiC) and porosity. The results on the composite grain models with inclusions of SiC show a longward shift in the $10\mu\text{m}$ absorption feature with the volume fraction of the inclusions whereas the composite grain models with graphite inclusions show a shortward shift in the $10\mu\text{m}$ feature. The $18\mu\text{m}$ feature, however, remains unaffected with variation in the volume fraction of the inclusions. The composite grain models with graphite inclusions were also used by Henning & Stognienko (1993) and they did not find any appreciable shift in the $10\mu\text{m}$ feature with inclusions, while Min et al. (2007) have found that it shifts shortwards. Our results on the porous silicate grains do not show any shift either in the 10 or the $18\mu\text{m}$ feature. Li et al. (2008) have used porous silicate grain models to study the $10\mu\text{m}$ feature in the AGNs and found that the $10\mu\text{m}$ peak shifts towards longer wavelength. For an elaborate comparison of models/results on silicate IR emission features see e.g. Kessler-Silacci et al. (2006) and Vaidya & Gupta (2011).

(2) We have also found that the composite grain models with the SiC inclusions modify the absorption profile in the spectral region 5 – $25\mu\text{m}$ and the $10\mu\text{m}$ silicate feature and do not fit M-type stars. This is consistent with the results obtained by Smolders et al. (2012)). These results on the composite grain models with SiC inclusions may be also compared with the C-rich stars with silicate emission features at 10 and $18\mu\text{m}$ as suggested by Little-Marenin (1986) & Smolders et al. (2012). We find that the shape of the SiC feature at $11.3\mu\text{m}$ varies with the shape of the grain. This is in agreement with the result obtained by Min et al. (2008).

Table 3. Variation of the flux ratio $R = \text{Flux}(18\mu)/\text{Flux}(10\mu)$ for various temperatures for SiC inclusions with DDA and EMA-T-Matrix models.

T(K)	DDA	EMA-T-Matrix
200	0.501	0.702
240	0.310	0.397
280	0.221	0.266
320	0.173	0.198
360	0.144	0.156
400	0.124	0.133

We note here that the composite grain models with the inclusions of graphite or SiC do not seem to fit well the selected sample of Spitzer stars. We need to analyze larger sample of M-type and AGB stars observed by Spitzer.

(3) We have found that the composite grain models with number of dipoles $N=14440$ ($AR=2.0$) and graphite inclusions with the volume fractions between 0.1 and 0.3 provide better fit than either with SiC inclusions or porous silicate grains for the selected IRAS stars (see Tables 1 and 2). Smolders et al. (2012) have used silicates and gehlenite to fit the observed 10 and $18\mu\text{m}$ silicate features and have also noted that grain models with a component of SiC may not fit the observed silicate features to the M-type stars. The IRAS 17423-1755 is an O-rich AGB star and it too does not fit well with grain models with SiC inclusion (see more on this AGB star in Manteiga et al. (2011)).

(4) The composite grain models with graphite and SiC inclusions and porous silicates give dust temperatures in the range 250–400K, which fit most of the observed IRAS-LRS curves selected for this paper. This temperature range compares well with the temperature range suggested by Bowey & Adamson (2001) and Voshchinnikov & Henning (2008). For stars giving good fits with composite grain models with graphite & SiC inclusions have dust temperature range between 270 and 300K, while for those giving good fits with porous models, have higher dust temperatures between 300 and 370K. The error in temperature estimates is within 10K.

(5) Flux ratios R is in the range from 0.15 to 0.25 in the dust temperature range of 250–300K, obtained for the composite grain models with graphite & SiC inclusions and porous silicate grain models compare well with the observed ratio. These values are lower than that given by Ossenkopf et al. (1992), which are in the range 0.30 to 0.60. The low value of R may be due to O-deficient silicates as noted by Little-Marenin & Little (1990) and Ossenkopf (1991). Most of the stars have the best fit flux ratio $R \sim 0.15\text{--}0.20$ for all the composite grain models.

The present study can be extended to Class 12 IRAS objects Gupta et al. (2004) which show similar but weaker silicate emission features at $10\mu\text{m}$. These results on the composite grain models and earlier studies Little-Marenin (1986) and Waters et al. (1998) clearly indicate that the composite grain models with other carbonaceous materials (e.g. amorphous silicates & amorphous carbon, ices & PAHs) as inclusions are required to interpret the observed IR emission from the circumstellar dust around O-rich as well as C-rich stars, to obtain more exact composition, sizes and shapes of the silicate grains in the circumstellar dust.

We also note that the optical constants for other carbonaceous materials by laboratory studies are required.

ACKNOWLEDGMENTS

D. B. Vaidya thanks IUCAA for funding the visits for completion of this work. The research has made use of the SIMBAD database, operated at CDS, Strasbourg, France.

REFERENCES

- Aitken D. K., Roche P. F., Spenser P. M., Jones B., 1979, *ApJ*, 233, 925
- Backman D. E., Witteborn F. C., Gillett F. C., 1992, *ApJ*, 385, 670
- Bazell D., Dwek E., 1990, *ApJ*, 360, 142
- Bode M. F., 1988, in Bailey M. E., Williams D. A., eds, *Dust in the Universe Observations and modelling of circumstellar dust*, pp 73–102
- Bohren C. F., Huffman D. R., 1983, *Absorption and scattering of light by small particles*. New York: Wiley, 1983
- Bowey J. E., Adamson A. J., 2001, *MNRAS*, 320, 131
- Brownlee D. E., 1987, in Hollenbach D. J., Thronson Jr. H. A., eds, *Interstellar Processes Vol. 134 of Astrophysics and Space Science Library*, Interstellar grains in the solar system. pp 513–530
- Carciofi A. C., Bjorkman J. E., Magalhães A. M., 2004, *ApJ*, 604, 238
- Chýlek P., Videen G., Geldart D. J. W., Dobbie J. S., Tso H. C. W., 2000, *Effective Medium Approximations for Heterogeneous Particles*. Academic Press, San Diego, USA
- Cohen M., 1984, *MNRAS*, 206, 137
- Draine B. T., 1988, *ApJ*, 333, 848
- Draine B. T., 2003, *ApJ*, 598, 1017
- Draine B. T., Flatau P. J., 2003, *ArXiv Astrophysics e-prints*
- Draine B. T., Lee H. M., 1984, *ApJ*, 285, 89
- Draine B. T., Li A., 2007, *ApJ*, 657, 810
- Greenberg J. M., 1990, *The evidence that comets are made of interstellar dust*. Kluwer Academic Publishers, Dordrecht, The Netherlands, pp 99–120
- Groenewegen M. A. T., 1997, *A&A*, 317, 503
- Gupta R., Mukai T., Vaidya D. B., Sen A. K., Okada Y., 2005, *A&A*, 441, 555
- Gupta R., Singh H. P., Volk K., Kwok S., 2004, *VizieR Online Data Catalog*, 215
- Henning T., Stognienko R., 1993, *A&A*, 280, 609

- Houck J. R., Roellig T. L., van Cleve J., Forrest W. J., Herter T., Lawrence C. R., Matthews K., Reitsema H. J., Soifer B. T., and others 2004, *ApJS*, 154, 18
- Iati M. A., Giusto A., Saija R., Borghese F., Denti P., Cecchi-Pestellini C., Aiello S., 2004, *ApJ*, 615, 286
- Kessler-Silacci J., Augereau J.-C., Dullemond C. P., Geers V., Lahuis F., Evans II N. J., van Dishoeck E. F., Blake G. A., Boogert A. C. A., Brown J., Jørgensen J. K., Knez C., Pontoppidan K. M., 2006, *ApJ*, 639, 275
- Kim S.-H., Martin P. G., 1995, *ApJ*, 444, 293
- Kirchschrager F., Wolf S., 2014, *A&A*, 568, A103
- Köhler M., Mann I., 2004, *J. Quant. Spec. Radiat. Transf.*, 89, 453
- Krivov A. V., Mann I., Krivova N. A., 2000, *A&A*, 362, 1127
- Lasue J., Botet R., Lévassieur-Regourd A. C., Hadamcik E., 2009, *Icarus*, 203, 599
- Lebouteiller V., Barry D. J., Goes C., Sloan G. C., Spoon H. W. W., Weedman D. W., Bernard-Salas J., Houck J. R., 2015, *ApJS*, 218, 21
- Lévassieur-Regourd A., Hadamcik E., 2013, in *AAS/Division for Planetary Sciences Meeting Abstracts Vol. 45 of AAS/Division for Planetary Sciences Meeting Abstracts, Properties of dust in inner cometary comae from polarimetric observations*. p. 505.02
- Li A., Greenberg J. M., 1998, *A&A*, 331, 291
- Li M. P., Shi Q. J., Li A., 2008, *MNRAS*, 391, L49
- Little-Marenin I. R., 1986, *ApJ*, 307, L15
- Little-Marenin I. R., Little S. J., 1990, *AJ*, 99, 1173
- Lorenz-Martins S., Lefevre J., 1993, *A&A*, 280, 567
- Manteiga M., García-Hernández D. A., Ulla A., Manchado A., García-Lario P., 2011, *AJ*, 141, 80
- Mathis J. S., 1996, *ApJ*, 472, 643
- Mathis J. S., Rumpl W., Nordsieck K. H., 1977, *ApJ*, 217, 425
- Min M., Hovenier J. W., de Koter A., Waters L. B. F. M., Dominik C., 2005, *Icarus*, 179, 158
- Min M., Hovenier J. W., Waters L. B. F. M., de Koter A., 2008, *A&A*, 489, 135
- Min M., Waters L. B. F. M., de Koter A., Hovenier J. W., Keller L. P., Markwick-Kemper F., 2007, *A&A*, 462, 667
- Mishchenko M. L., Travis L. D., Lacis A. A., 2002, *Scattering, absorption, and emission of light by small particles*. Cambridge University Press, UK
- O'Donnell J. E., 1994, *ApJ*, 437, 262
- Olton F. M., Raimond E., Neugebauer G., van Duinen R. J., Habing H. J., Aumann H. H., Beintema D. A., and others 1986, *A&AS*, 65, 607
- Ossenkopf V., 1991, *A&A*, 251, 210
- Ossenkopf V., Henning T., Mathis J. S., 1992, *A&A*, 261, 567
- Pegourie B., 1988, *A&A*, 194, 335
- Perrin J.-M., Lamy P. L., 1990, *ApJ*, 364, 146
- Perrin J.-M., Sivan J.-P., 1990, *A&A*, 228, 238
- Purcell E. M., Pennypacker C. R., 1973, *ApJ*, 186, 705
- Saija R., Iati M. A., Borghese F., Denti P., Aiello S., Cecchi-Pestellini C., 2001, *ApJ*, 559, 993
- Siebenmorgen R., Voshchinnikov N. V., Bagnulo S., 2014, *A&A*, 561, A82
- Simpson J. P., 1991, *ApJ*, 368, 570
- Smolders K., Neyskens P., Blommaert J. A. D. L., Hony S., van Winckel H., Decin L., van Eck S., Sloan G. C., Cami J., Uttenthaler S., Degroote P., and others 2012, *A&A*, 540, A72
- Sylvester R. J., Skinner C. J., Barlow M. J., Mannings V., 1996, *MNRAS*, 279, 915
- Telesco C. M., Knacke R. F., 1991, *ApJ*, 372, L29
- Vaidya D. B., Gupta R., 1997, *A&A*, 328, 634
- Vaidya D. B., Gupta R., 2009, *J. Quant. Spec. Radiat. Transf.*, 110, 1726
- Vaidya D. B., Gupta R., 2011, *A&A*, 528, A57
- Vaidya D. B., Gupta R., Dobbie J. S., Chylek P., 2001, *A&A*, 375, 584
- Vaidya D. B., Gupta R., Snow T. P., 2007, *MNRAS*, 379, 791
- Voshchinnikov N. V., Das H. K., Yakovlev I. S., Il'in V. B., 2013, *Astronomy Letters*, 39, 421
- Voshchinnikov N. V., Henning T., 2008, *A&A*, 483, L9
- Voshchinnikov N. V., Il'in V. B., Henning T., 2005, *A&A*, 429, 371
- Voshchinnikov N. V., Il'in V. B., Henning T., Dubkova D. N., 2006, *A&A*, 445, 167
- Waters L. B. F. M., Beintema D. A., Zijlstra A. A., de Koter A., Molster F. J., Bouwman J., de Jong T., Pottasch S. R., de Graauw T., 1998, *A&A*, 331, L61
- Werner M. W., Roellig T. L., Low F. J., Rieke G. H., Rieke M., Hoffmann W. F., Young E., Houck J. R., and others 2004, *ApJS*, 154, 1
- Whittet D. C. B., 2003, *Dust in the galactic environment*. Institute of Physics (IOP) Publishing, 2003 Series in Astronomy and Astrophysics, ISBN 0750306246, Bristol
- Wolff M. J., Clayton G. C., Gibson S. J., 1998, *ApJ*, 503, 815
- Wolff M. J., Clayton G. C., Martin P. G., Schulte-Ladbeck R. E., 1994, *ApJ*, 423, 412
- Wolf N. J., 1973, in *Greenberg J. M., van de Hulst H. C., eds, Interstellar Dust and Related Topics Vol. 52 of IAU Symposium, Circumstellar Infrared Emission. I the Circumstellar Origin of Interstellar Dust (review)*. p. 485
- Wolf N. J., Ney E. P., 1969, *ApJ*, 155, L181
- Zubko V., Dwek E., Arendt R. G., 2004, *ApJS*, 152, 211